Eur. Phys. J. Spec. Top.
https://doi.org/10.1140/epjs/s11734-024-01345-6

THE EUROPEAN PHYSICAL JOURNAL SPECIAL TOPICS

Regular Article

A brain-network operator for modeling disease: a first data-based application for Parkinson's disease

Maria Mannone[1,2,3,4,5,a], Peppino Fazio[4,6], Jürgen Kurths[2,3], Patrizia Ribino[1], and Norbert Marwan[2,3,7]

[1] ICAR, National Research Council (CNR), Rome, Italy
[2] Institute of Physics and Astronomy, Universität Potsdam, Potsdam, Germany
[3] Potsdam Institute for Climate Impact Research (PIK), Member of the Leibniz Association, Potsdam, Germany
[4] DSMN, Università Ca' Foscari di Venezia, Venice, Italy
[5] ECLT, Università Ca' Foscari di Venezia, Venice, Italy
[6] Department of Telecommunications, VSB - Technical University of Ostrava, Ostrava, Czechia
[7] Institute of Geosciences Potsdam, Universität Potsdam, Potsdam, Germany

Received 29 April 2024 / Accepted 16 September 2024

Abstract The complexity of our brains can be described as a multi-layer network: neurons, neural agglomerates, and lobes. Neurological diseases are often related to malfunctions in this network. We propose a conceptual model of the brain, describing the disease as the result of an operator affecting and disrupting the network organization. We adopt the formalism of operators, matrices, and tensor products adapted from theoretical physics. This novel approach can be tested and instantiated for different diseases, balancing mathematical formalism and data-driven findings, including pathologies where aging is included as a risk factor. We quantitatively model the K-operator from real data of Parkinson's Disease, from the Parkinson's Progression Markers Initiative (PPMI) upon concession by the University of Southern California. The networks are reconstructed from fMRI analysis, resulting in a matrix acting on the healthy brain and giving as output the diseased brain. We finally decompose the K-operator into the tensor product of its submatrices and we are able to assess its action on each region of interest (ROI) characterizing the brain for the specific considered samples. We also approximate the time-dependent K-operator from the fMRI of the same patient at the baseline and at the first follow-up. Our results confirm the findings of the literature on the topic. Also, these applications confirm the feasibility of the proposed analytic technique. Further research developments can compare operators for different patients and for different diseases, looking for commonalities and aiming to develop a comprehensive theoretical approach.

1 Introduction

Magic? No, Physics. Given a (non)magic formula, a variety of phenomena can be described, modeled, understood, and eventually modified. In particular, tools, such as random graphs, Markov graphs, small-world models, network-growth models, i.e., approaches to complex networks, can help model and understand the structure and organization of living and artificial networks [1]. Networks can describe the nature outside us and inside us, including our brains, from anatomy to functioning. For instance, the understanding of processes, such as a disease spread, can also be pursued by means of concepts from complex systems theory, such as percolation [2]. Network theory, jointly with graph theory and topology, is shedding new light in the field of neuroscience [3]. The anatomic and physiological architecture of our minds can be investigated for instance through complex networks. The knowledge of their nature may lead to technological developments, such as artificial intelligent systems (as multi-layer perceptrons), or foster new therapeutic insights. In fact, in the brain, there are regions characterized by a high connectivity, called *hubs* [4]. The pathological or surgical rescission of specific pathways can lead to macroscopic effects, dramatically affecting the life of patients. It is the case of the disconnection syndrome [5], with effects such as apraxia or aphasia, or even prosopagnosia, that is, the incapability of recognizing faces [6]. The alteration of weights in pathways can lead to psychiatric effects in schizophrenia [7]. The exaggeration of physiological mechanisms of activation and

[a] e-mails: maria.mannone@icar.cnr.it; maria.mannone@uni-potsdam.de (corresponding author)

Published online: 07 October 2024

inhibition of neurons, and their patterns of synchronization, fundamental also for healthy-brain music listening and appreciating [8], can lead to neural-masses synchronization in epileptic seizures [9–13]. It has been found a correspondence between the seizures' onsets and terminations with the increase and diminution of weights in the brain network [14]. Alterations of the network are also visible in Alzheimer–Perusini's disease [12, 15–17], leading to dementia. Thus, different neurological diseases present a different configuration of brain-network alteration [18]. Aging itself can be a risk factor for neurological diseases such as Alzheimer–Perusini. Focusing on brain networks can shed light also on the mechanisms inside an aging brain.

Despite the high volume of experimental and quantitative studies on specific diseases, as pointed out in [19], what is missing is a general theoretical description. Let us consider the brain as a multi-layer network, whose layers are the neurons, their agglomerates, and the lobes. In a recent study, we have proposed a novel, physics-inspired, conceptual model of neurological disease as the effect of an operator acting on the brain network and changing the weights of the connections between neural agglomerates [20]. The modularity of this brain description allows us to investigate diseases also in modular terms. We can build a conceptual model of neurological disease based on a suitable form of the K-operator (from *Krankheit*, German for *disease*) acting at different levels of the brain network. In our conceptual model, the K-operator acts differently on different brain regions, according to the position, typology, and level of introduced damage. For this reason, K can be written as the tensor product of its submatrices representing a different action on the different brain regions [20].

The disruption described by K can be compared with abnormal effects of communication between neural agglomerates. In addition, from a telecommunication point of view, a group of cells that work correctly but interrupt the transmission of the signal is equivalent to a group of cells that stop working. Thus, we can develop a model of network channel to describe the interaction between neural agglomerates in a general way, instantiating the effect of a particular disease in terms of disturbances of such a communication channel [20].

However, the conceptual model proposed in [20] has never been applied yet to real data from a neurological disease. In this article, we propose a technique to experimentally find a matrix shape of the K-operator starting from real human data, focusing in particular on Parkinson's Disease (PD). It is a progressive neurodegenerative disease, with severe sensory–motor and cognitive symptoms. From the literature, it is known that the network damage occurring in PD involves lower connectivity in corpus callosum, fornix, and cingulum, and higher connectivity between the left caudate and left medial frontal gyrus (orbital part), as well as a higher global connectivity after 36 months, probably due to compensatory processes [21]. In this study, we also start from the dataset considered in [21], focusing however on three selected persons: a healthy male control, a male PD patient, and a female PD patient. We obtain and compare their connectivity matrices, computing the K-operator. We also compute its inverse matrix form K^{-1}. Such a strategy could in principle suggest which brain-network regions should be addressed during therapy. In the second part of our research, we focus on the female PD patient, comparing her brain network at the baseline and at the first follow-up to approximate a time-dependent version of the K-operator.

This work is organized as follows. In Sect. 2, we present our strategy to compute an example of the K-operator as a data-driven matrix. Our results, with the analysis of two case studies, are presented in Sect. 3, and they are compared, looking for their similarities, in Sect. 5. A first, tentative contrasting example is proposed in Sect. 4, where we compare salient features of K for the passage from healthy to PD, to Alzheimer–Perusini's disease, and to schizophrenia. Finally, we summarize our research and its possible developments in Sect. 6.

2 Methods

Adopting the same notation as proposed in [20], we indicate here with $\mathcal{G}$ the block-matrix representing the weights of the connections in a healthy brain, where $\mathcal{G}$ stands for *Gehirn*, German for *brain*. This corresponds to a connectivity matrix with the information on precise weights. The letter K stands for the *Krankheit* (K) operator, whose action on $\mathcal{G}$ gives as output a diseased brain network: $\mathcal{G}^k = K\mathcal{G}$. From data, as it will be explained later in detail, we can obtain the connectivity matrix for brains of patients affected by a neurological disease, and of control people without the considered disease. If the matrix associated with $\mathcal{G}$ is invertible, we can experimentally derive a shape of K through Eq. (1)

$$K\mathcal{G} = \mathcal{G}^k \Rightarrow K = \mathcal{G}^k\mathcal{G}^{-1}. \tag{1}$$

In the following, we will be using the symbol $\mathcal{G}^p$ to indicate an instance of diseased brain affected by PD. To obtain a precise form for the matrices $\mathcal{G}$ and $\mathcal{G}^p$, we can start from medical measurements. The information on network physiology can be obtained through *Functional Magnetic Resonance Imaging* (fMRI), a technique of biomedical imaging detecting the variation of blood flow across the brain. The fMRI, formerly called *Nuclear Magnetic Resonance* (NMR), is a non-invasive yet highly informative strategy to retrieve information on the brain network. It provides information on functional brain activity [22]. From the physiological point of view, after having released oxygen into tissues, the blood contains deoxyhemoglobin, the molecule of hemoglobin without the

oxygen. This molecule presents a higher paramagnetism than tissues and, thus, it produces a stronger reaction to the magnetic resonance. Also, during the increment of activation of a neural region, the blood flow correspondingly increases[1] [22, 24].

fMRI are obtained with the same device needed for MRI. From the physics point of view, in these machines, a strong magnetic field forces the existing magnetic fields to align along it; since the alignment is imperfect, a precession motion starts. Then, a radio frequency pulse is applied; its energy is absorbed if it matches the resonance frequency of the precessing protons. Finally, the radio pulse is turned off, and the energy, released at different times, is measured, providing information on tissue organization and activity [22, 25].

The information collected via fMRI is encoded into a DICOM file, acronym for "Digital Imaging and COmmunications in Medicine." To obtain the connectivity matrices required for our research, we need an intermediate step of file conversion. In fact, DICOM is a rich format that has to be converted into a lighter format, shareable between different platforms for network-analysis purposes. Thus, we need a conversion from DICOM to NIfTI, acronym for "Neuroimaging Informatics Technology Initiative" [26]. In our research, to perform DICOM to NIfTI conversions, we use the Python library *dicom2nifti*,[2] and, to analyze data, the library *nilearn*[3] developed for applications of computational neuroscience.

The proportion-respecting visualization of the brain network requires the choice of a medical atlas for the anatomic distribution of the *regions of interest* (ROIs), the parts a brain can be divided into. This information does also determine the precise shape and size of the connectivity matrices. We will be working with matrices $N \times N$, where N is the total number of ROIs. We indicate with n, such that $n \in \{0, ..., N-1\}$, the index of the n-th ROI. Visually, each nm-th pixel represents the connectivity between the n-th and m-th part of the brain. For the *Multi-Subject Dictionary Learning* (MSDL) atlas [27], the brain is divided into $N = 39$ ROIs, listed in Table 1. The brain segmentation of the MSDL atlas is based on resting-state[4] fMRI (rs-fMRI) connectivity patterns, obtained by aggregating data from a great number of subjects [27].

Thus, the obtained connectivity matrices contain $39 \times 39 = 1521$ pixels, i.e., 1521 features.

The K-operator acts on the connectivity matrix. In our case studies, it will also have size 39×39 pixels. A possible grouping is the distinction of brain lobes (Table 2). For this first study, we considered the statistical information provided by MSDL atlas, as a preliminary investigation on the whole-brain information and in more detail on the diagonal blocks of K. For an additional investigation, to gain more information on the limbic system and its connections with other brain areas, we considered the third version of the automatic anatomic labeling atlas, that is, AAL3 [29], including 170 ROIs. The original AAL was developed at the Montreal Neurological Institute (MNI).[5] In our analysis, we included the 162 ROIs for which we have data (case study A) and 160 (case study B). In this way, we obtained matrices with 162×162 and 160×160 pixels, respectively. Table 3 shows the complete list of the considered ROIs from AAL3.

We can formally relate the brain $\mathcal{G}$, described by a connectivity matrix, to the groupings of submatrices. We adapt here the formalism of operators, matrix products, and tensor products, typically used for theoretical physics, to a problem of applied physics and neurology. Following the formalism proposed in [20], we treat the $\mathcal{G}$ as the composite system defined via the tensor product of its submatrices, the groupings of ROIs corresponding to the lobes

$$parietal \otimes frontal \otimes \ldots \otimes subcortical \rightarrow brain, \tag{2}$$

where $\otimes$ indicates the tensor product, that is, the *outer product*. Given two matrices a, b, indicating by b^t the transposed of the second matrix, their tensor product is defined as

$$a \otimes b := ab^t. \tag{3}$$

[1] The first intuition of the connection between blood-flood variation and brain activity is due to the Italian physiologist Angelo Mosso (1846–1910). His "human circulation balance," a non-invasive measure of blood redistribution during emotional and intellectual activity, is one of the first neuroimagining techniques [23].

[2] https://dicom2nifti.readthedocs.io/en/latest/.

[3] https://nilearn.github.io/stable/index.html.

[4] It indicates the resting-state functional magnetic resonance imaging (rsfMRI). This kind of data is acquired when the participant is supine or in a resting position with the right–left (RL) orientation. The resting-state fMRI provides information on spontaneous brain activity when the patient is not performing a specific task. The intrinsic brain networks and connectivity patterns are measured through blood oxygen level-dependent signals.

[5] https://www.oxcns.org/aal3.html.

Table 1 Regions of interest (ROIs) of the brain network according to the MSDL atlas [27]

ROI	Name
1	Left Auditory Cortex
2	Right Auditory Cortex
3	Striate Cortex
4	Left Default Mode Network
5	Medial Default Mode Network
6	Frontal Default Mode Network
7	Right Default Mode Network
8	Occipital Posterior
9	Motor Cortex
10	Right Dorsolateral Prefrontal Cortex
11	Right Frontopolar Cortex
12	Right Parietal Cortex
13	Right Posterior Temporal Cortex
14	Basal Ganglia
15	Left Parietal Cortex
16	Left Dorsolateral Prefrontal Cortex
17	Left Frontopolar Cortex
18	Left Intraparietal Sulcus
19	Right Intraparietal Sulcus
20	Left Lateral Occipital Complex
21	Visual Cortex
22	Right Lateral Occipital Complex
23	Dorsal Anterior Cingulate Cortex
24	Ventral Anterior Cingulate Cortex
25	Right Anterior Insula
26	Left Superior Temporal Sulcus
27	Right Superior Temporal Sulcus
28	Left Temporoparietal Junction
29	Broca's Area
30	Superior Frontal Sulcus
31	Right Temporoparietal Junction
32	Right Pars Opercularis
33	Cerebellum
34	Dorsal Posterior Cingulate Cortex
35	Left Insula
36	Cingulate Cortex
37	Right Insula
38	Left Anterior Intraparietal Sulcus
39	Right Anterior Intraparietal Sulcus

Table 2 Regions of interest (ROIs) of the brain network according to the MSDL atlas [27], ordered according to major brain areas. Here, the insula inside the "subcortical and other structures." However, it is sometimes indicated as a lobe itself [28]

Lobe	ROI	Name
Frontal	9	Motor (Motor Cortex)
	10	R DLPFC (Right Dorsolateral Prefrontal Cortex)
	16	L DLPFC (Left Dorsolateral Prefrontal Cortex)
	11	R front pole (Right Frontal Pole)
	17	L front pole (Left Frontal Pole)
	30	Sup Front S (Superior Frontal Sulcus)
	23	D ACC (Dorsal Anterior Cingulate Cortex)
	24	V ACC (Ventral Anterior Cingulate Cortex)
	32	R Pars Op (Right Pars Opercularis)
	7	R DMN (Right Default Mode Network)
	6	Front DMN (Frontal Default Mode Network)
	29	Broca (Broca's Area)
Temporal	1	L Aud (Left Auditory Cortex)
	2	R Aud (Right Auditory Cortex)
	4	L DMN (Left Default Mode Network)
	5	Med DMN (Medial Default Mode Network)
	26	L STS (Left Superior Temporal Sulcus)
	27	R STS (Right Superior Temporal Sulcus)
	13	R Post Temp (Right Posterior Temporal Lobe)
Parietal	28	L TPJ (Left Temporoparietal Junction)
	31	R TPJ (Right Temporoparietal Junction)
	12	R par (Right Parietal Cortex)
	15	L par (Left Parietal Cortex)
	19	R IPS (Right Intraparietal Sulcus)
	18	L IPS (Left Intraparietal Sulcus)
	38	L Ant IPS (Left Anterior Intraparietal Sulcus)
	39	R Ant IPS (Right Anterior Intraparietal Sulcus)
Occipital	3	Striate (Striate Cortex)
	8	Occ post (Occipital Posterior)
	20	L LOC (Left Lateral Occipital Complex)
	21	Vis (Visual Network)
	22	R LOC (Right Lateral Occipital Complex)
Subcortical and other structures	14	Basal (Basal Ganglia)

Table 2 (continued)

Lobe	ROI	Name
	25	R A Ins (Right Anterior Insula)
	33	Cereb (Cerebellum)
	34	Dors PCC (Dorsal Posterior Cingulate Cortex)
	36	Cing (Cingulate Cortex)
	35	L Ins (Left Insula)
	37	R Ins (Right Insula)

The action of the K-operator is similarly decomposed into its action on each lobe. Identifying $\mathcal{G}$ with the $N \times N$ connectivity matrix, we write

$$\begin{aligned}\mathcal{G} = &\mathcal{G}|_{n\in F}\otimes\mathbb{I}_{P,\,T,\,O,\,S} + \mathbb{I}_F \otimes \mathcal{G}|_{n\in P}\otimes\mathbb{I}_{T,\,O,\,S}\\ &+ \mathbb{I}_{F,\,P} \otimes \mathcal{G}|_{n\in T}\otimes\mathbb{I}_{O,\,S} + \mathbb{I}_{F,\,P,\,T} \otimes \mathcal{G}|_{n\in O}\otimes\mathbb{I}_S\\ &+ \mathbb{I}_{F,\,P,\,T,\,O} \otimes \mathcal{G}|_{n\in S},\end{aligned} \tag{4}$$

where F stands for frontal, P for parietal, T for temporal, O for occipital, and S for subcortical. The brain of patients affected by Parkinson's Disease, indicated as $\mathcal{G}^p$, can be decomposed in the same way.

With the connectivity matrices for the healthy and diseased brains, we can find the corresponding K-operator of Eq. (1) and its decomposition into submatrices acting on each ROI, and on each grouping of ROIs (4). Mathematically, the K-operator acts as a matrix product

$$\begin{aligned}K\mathcal{G} = &(K|_{n\in F}\otimes\mathbb{I}_{P,\,T,\,O,\,S})(\mathcal{G}|_{n\in F}\otimes\mathbb{I}_{P,\,T,\,O,\,S})\\ &+ \ldots = (K|_{n\in F}\mathcal{G}|_{n\in F}) \otimes \mathbb{I}_{P,\,T,\,O,\,S} + \ldots\end{aligned} \tag{5}$$

In [20], the product is defined as element-wise product, with each element of K acting as a multiplying factor to modify the corresponding element of the brain matrix. Here, we will consider both approaches, element-wise and usual matrix product. The tensor product symbol is adopted to formally extend the action of a submatrix of K on the whole matrix. While considering the element-wise product, the meaning of the identity is a matrix of 1s, that is, neutral elements as multiplicative factors. While considering the normal product, the identity is the usual identity matrix, having 1s on the main diagonal, and 0s elsewhere.

Our overall strategy to obtain the K-operator from patients' fMRI is summarized in the Pseudocode 1. To approximate the time evolution of the disease in an already-diseased brain, with a little abuse of notation, considering the brain matrices at each time point as independent matrices, we write

$$K(t)\mathcal{G}^p(t) = \mathcal{G}^p(t+1) \Rightarrow K(t) = \mathcal{G}^p(t+1)[\mathcal{G}^p(t)]^{-1}. \tag{6}$$

More refined techniques for time-evolution operator approximation can be applied to the K computed at different time-points, looking for a more general approximation of the time-dependent K-operator, and, through a suitable training and test, to potentially allowing one to make predictions on disease's progression. We will be using Eq. (1) and (6) to obtain our results, presented in Sect. 3. To obtain our network visualizations, we adapt the first part of a Graph Neural Network (GNN) developed at Stanford [30]. To compute the K-operator, here we can choose to treat K as acting element-wise on each element of the connectivity matrix

$$K^\delta\mathcal{G} = \mathcal{G}^\delta \Rightarrow \left\{K^\delta_{z,\,z'}c^l_{z,\,z'}\right\} = \left\{c^{l,\,\delta}_{z,\,z'}\right\}; \tag{7}$$

thus, we will be mostly using a element-wise product to find it, obtaining a symmetric shape for K, with its elements indicating the precise disease action on the corresponding pairs of ROIs. Further research will consider the rows–matrix product, and exploit a subsequent diagonalization to make the elements of K interpretable. To attempt a first comparison, we also computed K with the classic product. As it will be visible from the figures, vertical lines of K obtained via row-by-column product approximately correspond to clusters (regions of high variability) of K computed with the element-wise product. Thus, there seems to be a relationship in terms of patterns of variability.

Our matrix approach requires that the submatrices have all the same size. An alternative approach consists in the re-writing of the K-operator as a block-diagonal matrix, where each block corresponds to the action of K on

Table 3 The considered ROIs of the brain parcellation according to the AAL3 atlas [29]. The ROI position can be retrieved as $(n-1)$ the numbering associated with the labels

ROI label
Precentral_L 1
Precentral_R 2
Frontal_Sup_2_L 3
Frontal_Sup_2_R 4
Frontal_Mid_2_L 5
Frontal_Mid_2_R 6
Frontal_Inf_Oper_L 7
Frontal_Inf_Oper_R 8
Frontal_Inf_Tri_L 9
Frontal_Inf_Tri_R 10
Frontal_Inf_Orb_2_L 11
Frontal_Inf_Orb_2_R 12
Rolandic_Oper_L 13
Rolandic_Oper_R 14
Supp_Motor_Area_L 15
Supp_Motor_Area_R 16
Olfactory_L 17
Olfactory_R 18
Frontal_Sup_Medial_L
Frontal_Sup_Medial_R 20
Frontal_Med_Orb_L 21
Frontal_Med_Orb_R 22
Rectus_L 23
Rectus_R 24
OFCmed_L 25
OFCmed_R 26
OFCant_L 27
OFCant_R 28
OFCpost_L 29
OFCpost_R 30
OFClat_L 31
OFClat_R 32
Insula_L 33
Insula_R 34
Cingulate_Ant_L
Cingulate_Ant_R
Cingulate_Mid_L 37
Cingulate_Mid_R 38
Cingulate_Post_L 39

Table 3 (continued)

ROI label
Cingulate_Post_R 40
Hippocampus_L 41
Hippocampus_R 42
ParaHippocampal_L 43
ParaHippocampal_R 44
Amygdala_L 45
Amygdala_R 46
Calcarine_L 47
Calcarine_R 48
Cuneus_L 49
Cuneus_R 50
Lingual_L 51
Lingual_R 52
Occipital_Sup_L 53
Occipital_Sup_R 54
Occipital_Mid_L 55
Occipital_Mid_R 56
Occipital_Inf_L 57
Occipital_Inf_R 58
Fusiform_L 59
Fusiform_R 60
Postcentral_L 61
Postcentral_R 62
Parietal_Sup_L 63
Parietal_Sup_R 64
Parietal_Inf_L 65
Parietal_Inf_R 66
SupraMarginal_L 67
SupraMarginal_R 68
Angular_L 69
Angular_R 70
Precuneus_L 71
Precuneus_R 72
Paracentral_Lobule_L 73
Paracentral_Lobule_R 74
Caudate_L 75
Caudate_R 76
Putamen_L 77
Putamen_R 78
Pallidum_L 79
Pallidum_R 80
Thalamus_L

Table 3 (continued)

ROI label
Thalamus_R
Heschl_L 83
Heschl_R 84
Temporal_Sup_L 85
Temporal_Sup_R 86
Temporal_Pole_Sup_L 87
Temporal_Pole_Sup_R 88
Temporal_Mid_L 89
Temporal_Mid_R 90
Temporal_Pole_Mid_L 91
Temporal_Pole_Mid_R 92
Temporal_Inf_L 93
Temporal_Inf_R 94
Cerebellum_Crus1_L 95
Cerebellum_Crus1_R 96
Cerebellum_Crus2_L 97
Cerebellum_Crus2_R 98
Cerebellum_3_L 99
Cerebellum_3_R 100
Cerebellum_4_5_L 101
Cerebellum_4_5_R 102
Cerebellum_6_L 103
Cerebellum_6_R 104
Cerebellum_7b_L 105
Cerebellum_7b_R 106
Cerebellum_8_L 107
Cerebellum_8_R 108
Cerebellum_9_L 109
Cerebellum_9_R 110
Cerebellum_10_L 111
Cerebellum_10_R 112
Vermis_1_2 113
Vermis_3 114
Vermis_4_5 115
Vermis_6 116
Vermis_7 117
Vermis_8 118
Vermis_9 119
Vermis_10 120
Thal_AV_L 121
Thal_AV_R 122
Thal_LP_L 123

Table 3 (continued)

ROI label
Thal_LP_R 124
Thal_VA_L 125
Thal_VA_R 126
Thal_VL_L 127
Thal_VL_R 128
Thal_VPL_L 129
Thal_VPL_R 130
Thal_IL_L 131
Thal_IL_R 132
Thal_Re_L 133
Thal_Re_R 134
Thal_MDm_L 135
Thal_MDm_R 136
Thal_MDl_L 137
Thal_MDl_R 138
Thal_LGN_L 139
Thal_LGN_R 140
Thal_MGN_L 141
Thal_MGN_R 142
Thal_PuI_L 143
Thal_PuI_R 144
Thal_PuM_L 145
Thal_PuM_R 146
Thal_PuA_L 147
Thal_PuA_R 148
Thal_PuL_L 149
Thal_PuL_R 150
ACC_sub_L 151
ACC_sub_R 152
ACC_pre_L 153
ACC_pre_R 154
ACC_sup_L 155
ACC_sup_R 156
N_Acc_L 157
N_Acc_R 158
VTA_L 159
VTA_R 160
SN_pc_L 161
SN_pc_R 162
SN_pr_L 163

a lobe. The interaction elements, related to inter-lobes connectivity, disappear from this kind of visualization, in analogy with the original, simplified approach proposed in [20].

Algorithm 1 The proposed technique to compute data-driven examples of the K-operator

for fMRI in {healthy, diseased fMRIs} **do**:
    conversion DICOM→NIfTI,
    computation of the connectivity matrix (e.g., [0]) from the .nii file;
    computation of the 3D graph of the brain network from the connectivity matrix.
end for
store the diseased network as $\mathcal{G}^p$
store the healthy network as $\mathcal{G}$
if $\mathcal{G}$ is invertible and $\mathcal{G}^p$, $\mathcal{G}$ are of the same size **then**
    compute K as $K = \mathcal{G}^p\mathcal{G}^{-1}$
    for each region of interest **do**
        compute the submatrix of K acting on it
    end for
    write K as the tensor product of its submatrices
end if

3 Results

We apply the described methods (Sect. 2) to gain insights on the effect of Parkinson's Disease (PD) on the human functional brain network. According to Mayo's clinic,[6] "Parkinson's disease is a progressive disorder that affects the nervous system and the parts of the body controlled by the nerves." Symptoms start with a limited tremor in one hand. Other further symptoms, appearing with the worsening of the disease, involve speech speed, handwriting size, tremor, and rhythmic shaking, slow movement (bradykinesia), muscle stiffness, and loss of automatic movements. These symptoms can, thus, also be related with Broca's area for the speech [31], and parietal-frontal network and subcortical structures for the motor-movement execution [32]. We expect that the K-operator approach may highlight effects of the disease in these areas.

For our research, we consider the dataset Parkinson's Progression Markers Initiative (PPMI), collected by the Stevens Neuroimagining and Informatics Institute of the University of Southern California (USC). For our tests, we first consider an example of fMRI from a human control brain, and an example of fMRI from a brain of a human patient affected by PD. Then, we consider the fMRI at two different time-points, the baseline and the first follow-up, of the same patient. In fact, in this article, we are interested in the definition of a technique to relate the conceptual model of [20] with real data. With our choice of patients, we wanted to highlight the heterogeneity inside the same disease, looking for those common elements that could better characterize the disease at a more high-abstract way.

3.1 Case study A

In this first case study, we build a shape of the K-operator that transforms a healthy-brain network into a diseased one. We start with data from two patients, a healthy control and a diseased one. The healthy control is male, 73 years old; the PD patient is also male, 67 years old. Of both patients is considered the fMRI with the rsfMRI_RL technique.

The PD patient has been observed at the fourth visit (V04), that is, after 12 months from the baseline. We propose a visualization of the brain network via three projections: coronal, sagittal, and axial, respectively (Fig. 1 left, where the color indicates the intensity of the connectivity). To this aim, we adapt the initial part of a code from [30] (see the paragraph on *Codes availability*). Each pixel of the matrices (as heatmaps) represents a pair of regions of interest (ROI), whose list is given in Table 1.

Thus, we visualize both the control network and the diseased network, the corresponding connectivity matrices, and the data-derived K-operator in matrix form, with the additional visualization of its action on the brain regions. The K-operator can be decomposed into the tensor product of its submatrices acting on specific brain areas, as shown in Eq. (5). In particular, if we consider ROIs codified through medical atlases, the corresponding submatrix

[6] https://www.mayoclinic.org/diseases-conditions/parkinsons-disease/.

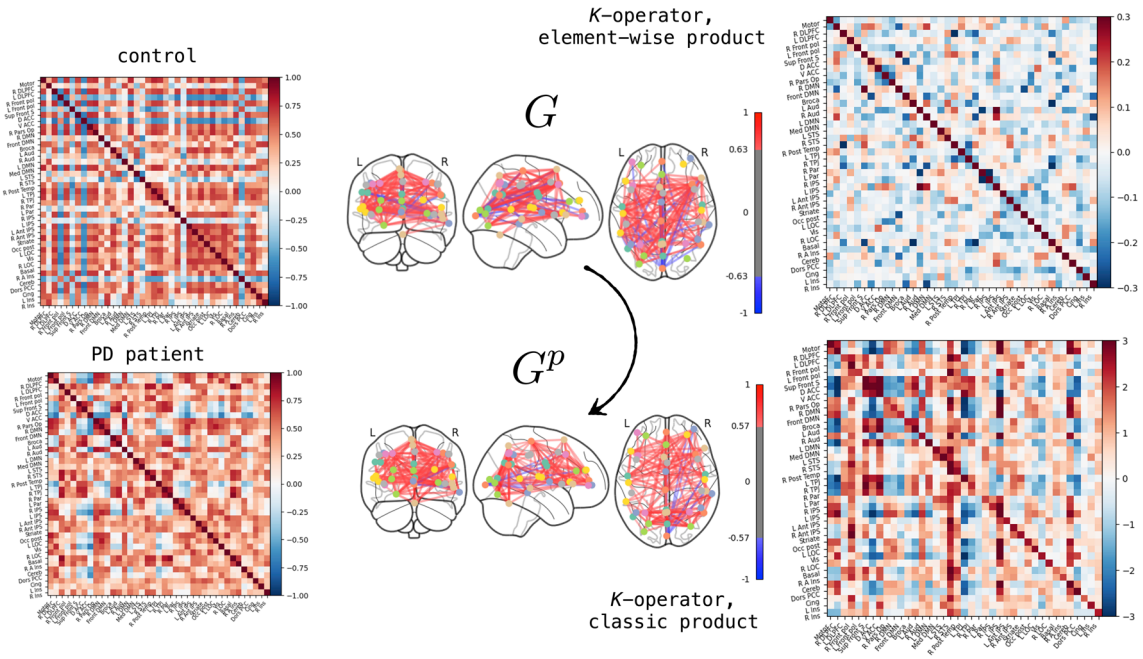

Fig. 1 Connectivity matrix and brain network of a healthy control and of a Parkinson's Disease patient, and the K-operator ideally transforming the healthy network into the diseased one. Here, the K-operator is computed from the connectivity matrices of a healthy control (male, 73 years old) and a PD patient (male, 67 years old). Colors indicate the intensity of the connectivity. The ROIs of K are re-ordered. We include the K-operator computed with the element-wise product, and with the row-by-colum (classic) product

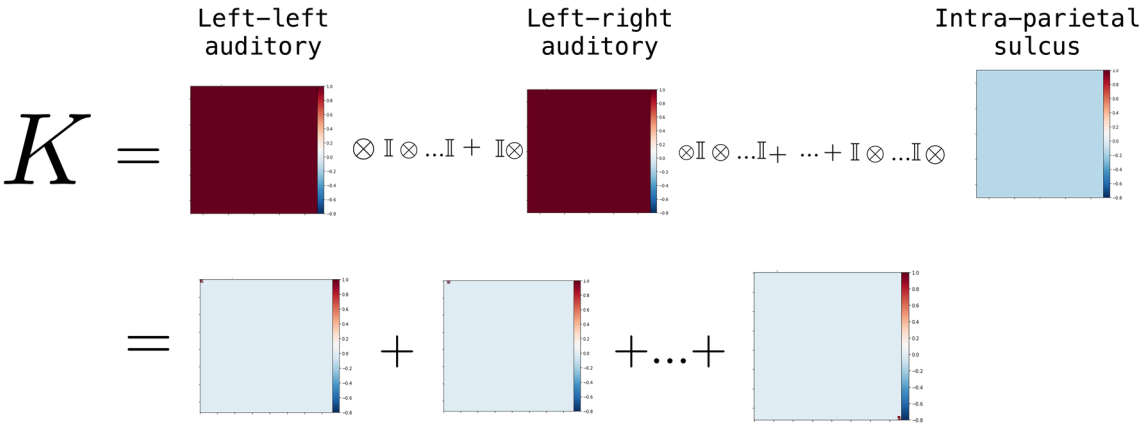

Fig. 2 Decomposition of the K-operator into the tensor product of its submatrices acting on each region of interest in the special case when the submatrices have dimension 1. The tensor product of each one-pixel submatrix and the identity matrices gives matrices having all elements zero except that pixel. Their sum gives back the K-operator. The decomposition follows the original order of the ROIs

is a number. A grouping of ROIs would lead to larger submatrices. The K-operator can be written as the sum of the matrices acting on each region $\otimes$ identity matrices for the other regions (Fig. 2).

We propose a decomposition of the K-operator where we group the ROIs (MSDL atlas) according to their belonging to the same lobe (Table 2), obtaining the representation of Fig. 3. In this case, it becomes fundamental to adjust the size of the identity matrices, given that the blocks of the K-operator have different size according to the number of ROIs that populate the lobes.

Let us now comment the information obtained on the K-operator action by observing Fig. 3.

In the **frontal lobe**, there is a high effect of decreased connectivity between the Dorsal Anterior Cingulate Cortex and the Ventral Anterior Cingulate Cortex. A decreased connectivity is also found in the literature [33]. An increase of connectivity is shown between the right frontal pole and the frontal default mode network. A

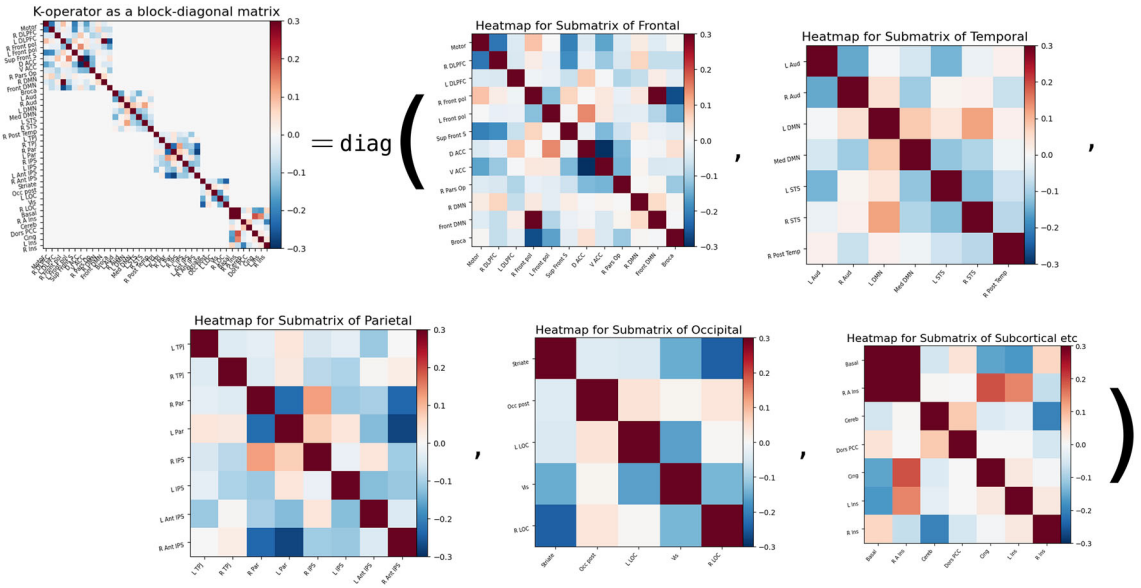

Fig. 3 The K-operator of Fig. 1 can be rewritten as a block-diagonal matrix, where the blocks are the submatrices corresponding to groupings of ROIs, re-ordered according to the lobes. This representation hides the interaction terms between different lobes, and, thus, it is related to the approach in [20]. Considering the lobes as groupings, we obtain the K-operator above. The following decomposition highlights the action of the K-operator onto frontal lobe, parietal lobe, temporal lobe, occipital lobe, and subcortical part of the human brain

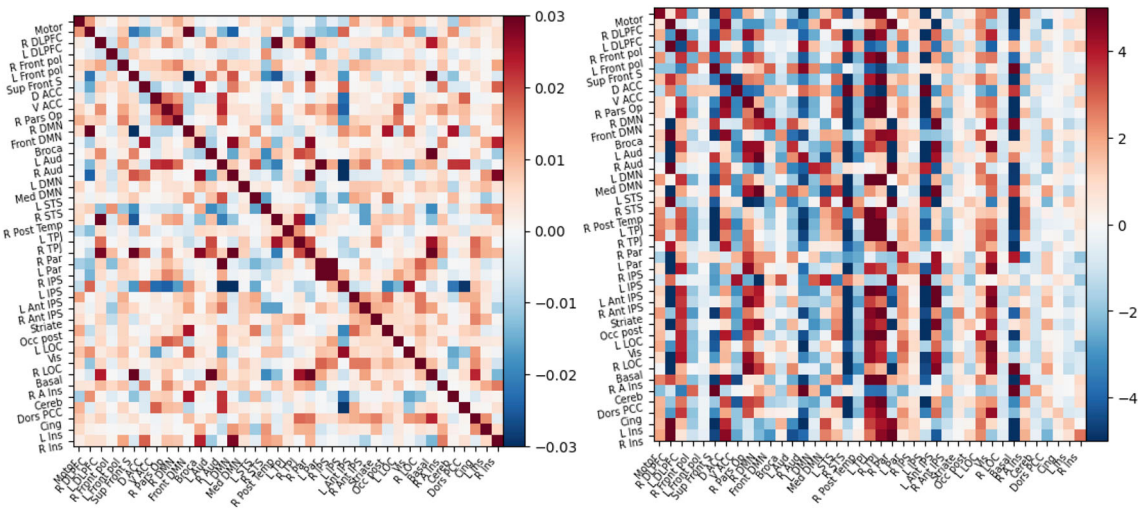

Fig. 4 The operator K^{-1}, corresponding to the "healing" for the considered case (left: element-wise product; right: row-by-column product)

decreased connectivity is found between the Broca's area and the right frontal pole. Studies on PD found that Broca's area is involved in speech issues related with the disease [31]. In the **parietal lobe**, there is a decrease in connectivity between the right anterior intraparietal sulcus and the left parietal cortex. Interestingly, there is a a discussion on the role of right superior parietal cortex and the intraparietal sulcus concerning letters recognition and their damage for PD patients [34]. We also notice an increase in connectivity between the basal ganglia and the right anterior insula, inside **subcortical structures**. The alteration of basal ganglia in Parkinson's Disease is responsible of motor dysfunction [35]. Disruptions involve the right pars opercularis, the left and right insula, the right temporo-parietal junction, and the left anterior intraparietal sulcus. Thus, our results seem to confirm recent studies on PD that, starting from the comparison between fMRI of healthy control and PD patients, found variations inside insula, frontal, cingulate and temporal cortex, and temporal lobes [21].

In addition, we also compute K^{-1} operator for the considered example (Fig. 4 left). The inverse of the K-operator should correspond to the *therapy*, the *Operation* operator as described in [20]: a mixture of surgery, therapeutical intervention, and possible new techniques to ideally lead to a complete healing of the patient. It is particularly evident the need for an action to strengthen the connectivity of the lateral occipital cortex (L LOC), to decrease the connectivity of the right hemisphere counterpart of the intraparietal sulcus (R IPS), for a mixed action on the right auditory side (R Aud), and on the dorsal (or posterior) part of the posterior cingulate cortex (Dors PCC). Computing K^{-1} with the classic technique, we notice in particular a vertical correspondence with left dorsolateral prefrontal cortex, cingulate cortex, basal ganglia, intraparietal sulcus, right default mode network, and lateral occipital cortex.

We also computed the K-operator with respect to the AAL3 atlas; see Fig. 5. For case study B, we had to exclude substantia nigra for lack of the corresponding voxels according to the NIfTI file. For the sake of readability of the image, we imposed an empiric threshold on the values of K to be shown, leaving only the points of major impact of the disease. We notice a correspondence between the vertical agglomerates of row-by-column K with the clusters of element-wise K. We choose to focus on the limbic system and substantia nigra. The latest has a major role in PD, given the defect of dopamine release, and dopaminergic circuit, also involving striatus and ventral tegmental area (VTA). From Fig. 5 (down), we notice a variation of connectivity between the substantia nigra pars compacta, Thal_Pul_R (pulvinar right), and nucleus accumbens. Considering substantia nigra pars compacta, we notice a connectivity variation with Thalamus_VA_R (ventral anterior), VL_L (ventral lateral left), VL_R (ventral lateral right), cerebellum 10-R, and between nucleus accumbens and cerebellum crus 1R, and between VTA and cerebellum crus 2 L. In particular, we find an increase of connectivity between VTA and nucleus accumbens left. Cerebellar connectivity alterations with substantial nigra and VTA are confirmed in the literature, and in particular, an increase of connectivity between VTA and right cerebellum [36, 37].

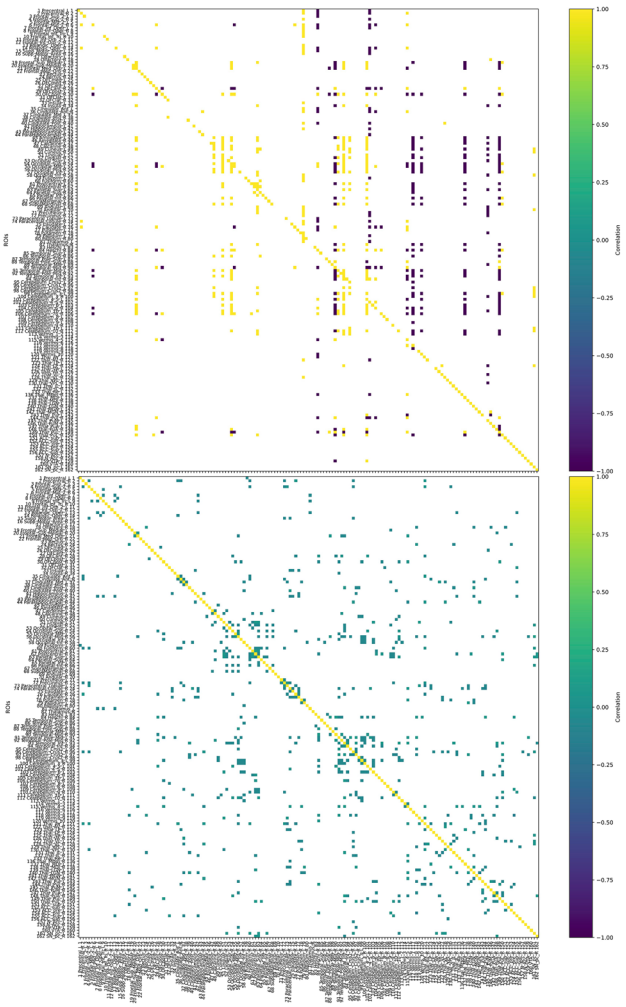

Fig. 5 K-operator computed for case A according to the AAL3 atlas, with more details including parts of the cerebellum and limbic system. Top: K according to the row-by-column product (threshold 1.8); down: K according to the element-wise product (threshold: 0.04)

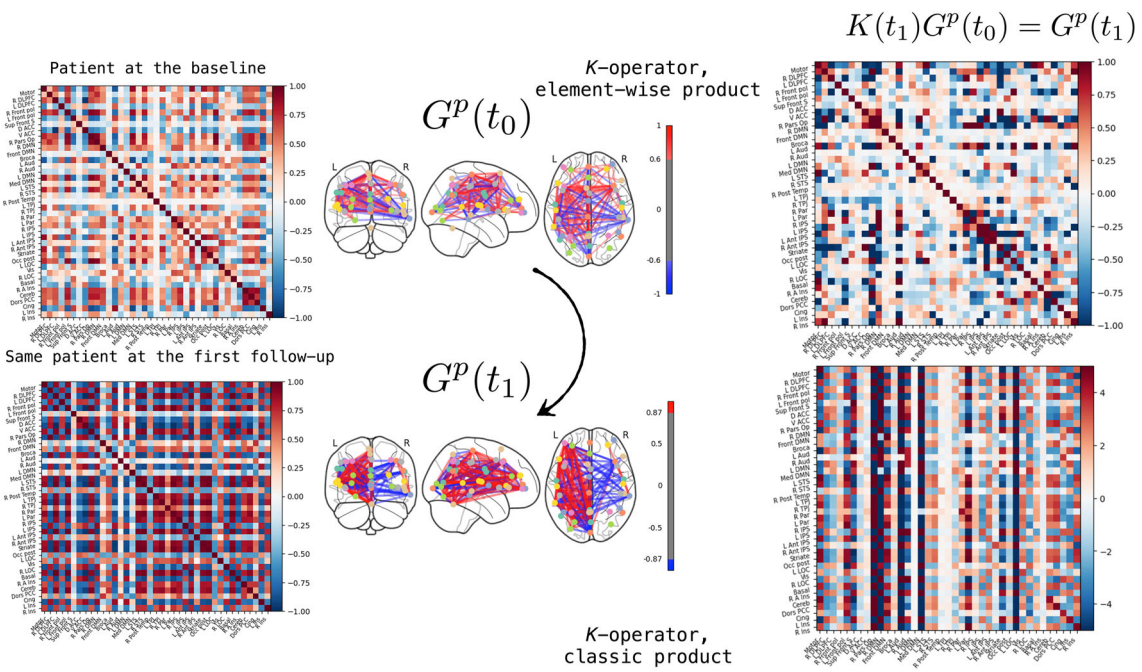

Fig. 6 K-operator leading the evolution of PD in the same patient, a female PD patient, from the baseline to the first follow-up

3.2 Case study B

In this second case study, we compute a shape of the K-operator constituting the time evolution of a PD–brain network.

We examined the fMRI of the same patient from the baseline (time t_0) to the first follow-up (time t_1), 1 year later. Our second test provides insights on the time-dependency of the K-operator. The connectome at both time-points is shown in Fig. 6. Being interested in testing the method, as well as finding disease-related key features, we focused on two case studies that were different between them. In particular, the time evolution was investigated in a relatively young female patient to exclude age effects, and diversifying the research with respect to case study A (with connectomes of a healthy male and a diseased male). The selected patient is female, of 56 years old at the baseline. We considered also in this case the rsfMRI_RL. We compute here the K operator at time t_1, that is

$$K(t_1)G^p(t_0) = G^p(t_1). \tag{8}$$

Observing the lobe-decomposition of the K-operator (Fig. 7), we notice an agreement with former literature. The color scale is increased for the single lobes to make the changes more evident, and decreased on the overall K-operator to make the overall organization more evident.

In the **frontal lobe**, a visible damage can be observed through the right and left dorsolateral prefrontal cortex, the motor area, and the Broca's area, whose effects of decreased connectivity have already been discussed also for the first case study. The dorsolateral prefrontal cortex is considered as one of the target regions where treatment, in form of transcranial magnetic stimulation, can reveal some positive effects, improving patients' performance in cognitive tasks [38]. Connectivity variation on the motor cortex have already been commented also for the first case study. We notice an increased connectivity between the dorsolateral prefrontal cortex and the frontopolar cortex (frontal pole). The alteration (even though a disruption) of their connection is considered as one of the markers of PD progression in the literature [39]. Concerning the **temporal lobe**, there is a decrease of connectivity between the left and the right superior temporal sulcus. From the overall K, an increase of connectivity between these two regions and the right anterior insula is visible.

In the **parietal lobe**, there are variations of connectivity throughout the lobe, for instance between the left intraparietal sulcus and the left parietal cortex, the right intraparietal sulcus, and the right anterior intraparietal sulcus. Connectivity changes also interest the temporo-parietal junction. A damage consisting in the progressive thickening of the gray matter in the temporo-parietal junction is found in a longitudinal study on PD [40]; thus, we can infer a connection between our functional-derived information and a time-dependent anatomic variation. An effect of PD on action and emotion perception is related with decreased activity concerning the left parietal cortex,

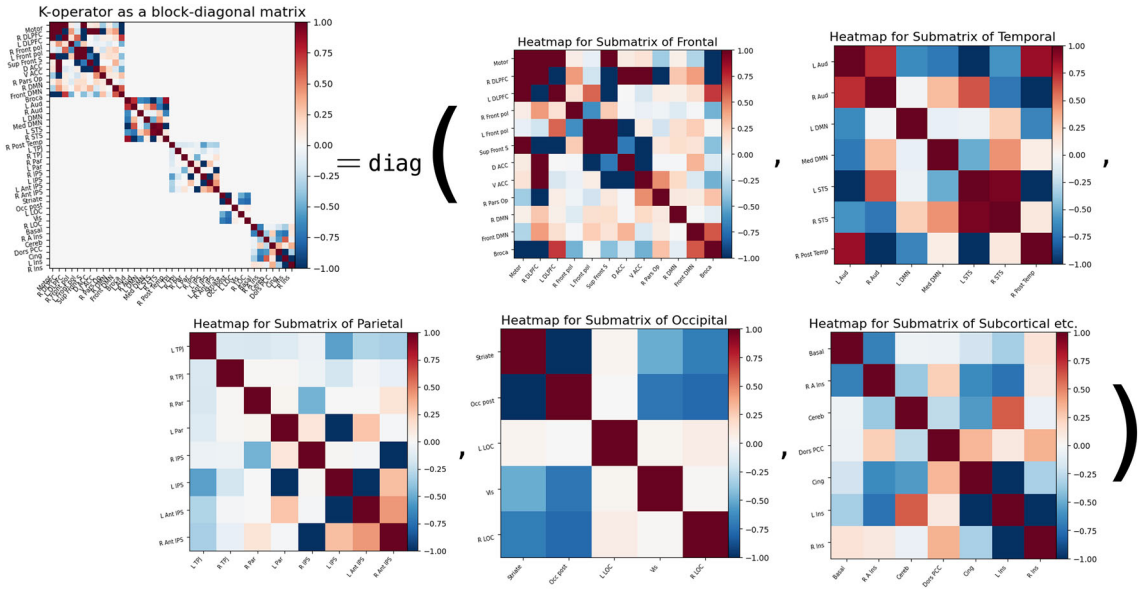

Fig. 7 Decomposition of the K-operator into submatrices acting on groupings of ROIs, neglecting the interaction terms, and re-ordering the ROIs. Here, the K-operator shows the disease evolution from the baseline to the first follow-up in a female patient of 56 years old. The blocks have been highlighted manually. The scale adopted to visualize the K-operator, enhancing details, ranges from -1 to 1

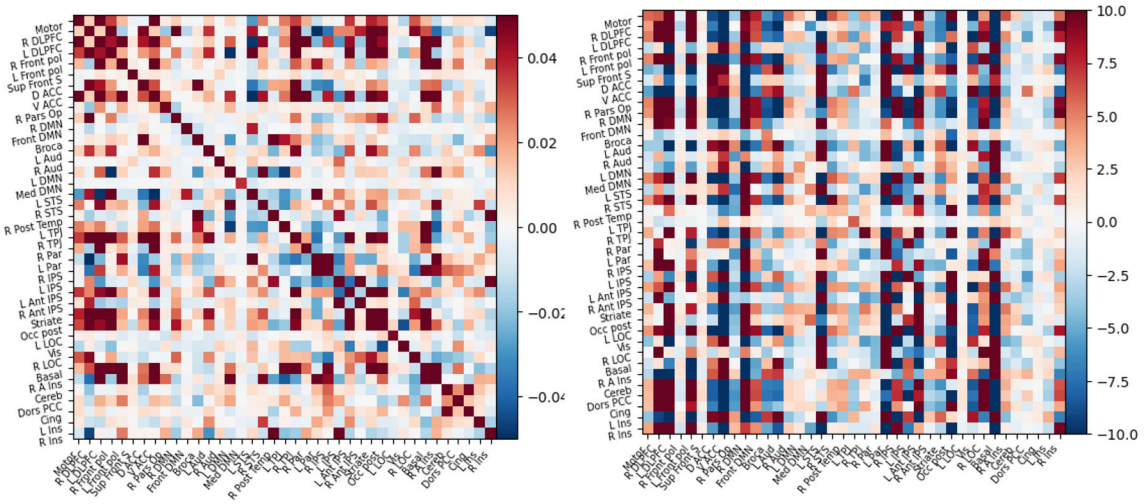

Fig. 8 The operator K^{-1}, corresponding to the "healing" for the second case study (left: with the element-wise product; right: with the column-by-matrix product). The scale is modified to make details more evident

in particular the intraparietal sulcus [41]. Disruptions in the **occipital lobe** mostly interest the decreased connectivity between the striate cortex, the occipital posterior, the visual network, and the right occipital complex. Visual dysfunctions are also found in PD patients, including allucinations [42]. Visual illusions are also associated with disruptions of the aforementioned intraparietal sulcus [43]. Also, for this second case study, we notice alterations of the connectivity between basal ganglia and right anterior insula (however concerning decreased connectivity), left insula, cerebellum, and cingulate. Alterations of the last one find a reference in the literature [44]. Finally, we notice an increase of connectivity between cerebellum and left insula. The healing operator, that is, K^{-1}, for this second case study is presented in Fig. 8.

Considering the AAL3 atlas, we can find some information on ventral tegmental area and nucleus accumbens. In particular, observing Fig. 9, and comparing K computed with both hybrid and classic techniques, we notice a correspondence of vertical agglomerates and clusters, envisaging the presence of patterns for the single patient and for the considered disease. Most highlighted areas include frontal, motor, angular, cuneus, putamen, temporal,

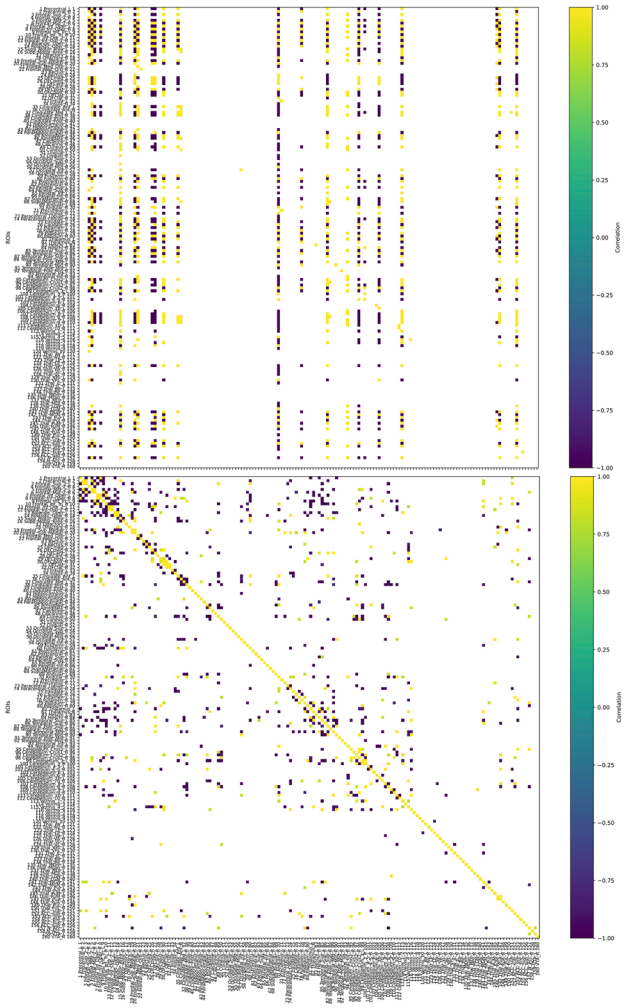

Fig. 9 K-operator computed for case B according to the AAL3 atlas. Top: K according to the row-by-column product (threshold 12); down: K according to the element-wise product (threshold: 0.5)

cerebellum, thalamus pulvinar, and nucleus accumbens. Focusing on the nucleus accumbens, we notice an increase of connectivity with middle frontal gyrus, cuneus, cerebellum crus 1 left, and VTA. The increase of connectivity between nucleus accumbens and ventral tegmental area is in line with the literature [36]. Interestingly, the authors of [37] do not confirm this information in their latest study, probably because of an effect of the age, altering the VTA connectivity. We also find a decrease of connectivity with the superior frontal gyrus (medial), anterior cingulate cortex, pallidum right, cerebellum 8R, and thalamus (mediodorsal medial). A dissociation between the midbrain connectivity (and in particular ventral tegmental area) and the right cerebellum is also found by [37] for PD patients, while expecting a lower connectivity between substantia nigra and right cerebellum. The authors of [37] mention a possible subsequent compensatory effect of VTA, strengthening the network, overcoming the damaged substantia nigra, and taking over cognitive functions as well. Thus, a reorganization of the network can act as a compensatory mechanism against cognitive decline [45, 46], happening at least in the first phases of the disease. Information on connectivity can be considered as a marker of risk of PD [47]. In fact, it has been shown that alterations of functional connectivity [47], and in particular of the connectivity between nucleus accumbens and anterior cingulate cortex, can precede apathy in PD patients [48]. The nucleus accumbens is connected with will and motivation; effects of PD on it, are related with psychiatric symptoms. The ventral tegmental area does also play a role for reward and motivation, being part of the dopaminergic network, thanks to its strong connection with the nucleus accumbens [36].

4 Contrasting example

Before discussing our results, we present here a preliminary comparison of the shapes that the K-operator can assume while modeling its action for different diseases. We present a graphic comparison of K computed between

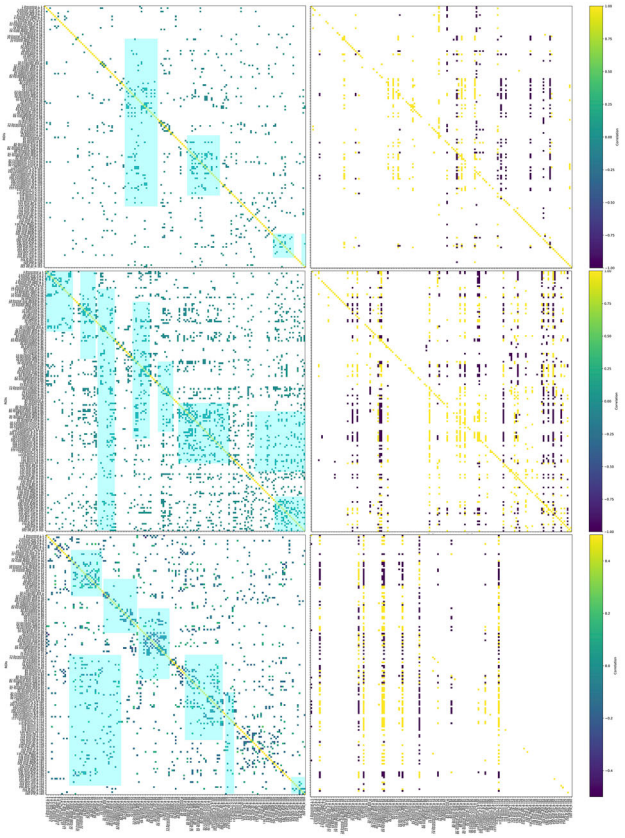

Fig. 10 Top: from left to right, K-operator (hybrid technique) between healthy controls and PD patient (left, threshold 0.04), schizophrenic patient (center, 0.03), and AD patient (right, 0.1). Bottom: same comparison, with K computed with the classic technique, with the respective thresholds equal to 1.8, 5, and 1.7

a healthy control and a PD patient (our case A), between a healthy control and an Alzheimer–Perusini's (AD) patient, and between an healthy control and a schizophrenic patient. The information on PD patient is derived from the ADNI 2 dataset,[7] and information on the schizophrenic patient from the COBRE dataset.[8] In Fig. 10, in addition to the already-discussed case A, we have K showing the brain-network changes occurring:

– between the same healthy control of PPMI (male, 74), and the patient A00015518 (male, 60), classified as schizophrenia_strict in the COBRE dataset, and
– between a 78-year-old CN female (ID: 018_S_4399), and a 73-year-old AD female (ID: 018_S_4696).

For our analysis, we consider the AAL3 atlas, for a higher focus on the limbic system. Observing the shape of the K-operator computed with both classic and hybrid techniques, and filtered to show only the highest values, we notice some characteristic features. For instance, in the passage from a healthy brain to a schizophrenic one, the role of amigdala is emphasized. However, further comparison with a higher number of patients is needed to draw more precise conclusions. For healthy→PD, K (hybrid computation) signals alterations mostly concerning temporal, fusiform, lingual, occipital, parietal, and supra marginal areas. For healthy→schizophrenic, disruption is mostly involving prefrontal area, thalamus, hippocampus, and Heschl gyrus, some of the areas more interested by the disease. Concerning healthy→AD, we notice a major effect of the disease on fusiform, thalamus, nucleus accumbens, ventral tegmental area, hippocampus, parahippocampal gyrus, orbitofrontal cortex, and occipital area. We also notice from K (classic computation) vertical clusters for healthy→AD mostly on parahippocampal gyrus and hippocampus, vermis, cerebellum 6R, parietal inferior, occipital, and frontal superior. Connectivity variations concerning substantia nigra, to a different extent, are present for all the three considered diseases, given the effects of dopamine imbalance.

[7] https://adni.loni.usc.edu/.
[8] https://www.nitrc.org/projects/schizconnect/.

5 Discussion

The two case studies, A (Sect. 3.1) and B (Sect. 3.2), cannot be straightforwardly compared, given differences in age and sex of the involved patients. For instance, we notice that the effects of the disease over time in a younger female patient seem to be higher than the effects found through the comparison between brain networks of a male healthy control and a male diseased patient both of older age. This difference is probably due to the aging effects on the brain, independently of the presence of the disease, and on functional differences due to sex. Further comparisons can lead to a more defined shape of the K-operator over time.

From the comparison of cases A and B, however, we can also spot some similarities, which may point toward more shared features of PD on functional brain networks. For case A, observing the *frontal lobe*, we notice a variation of connectivity between the right default mode network and the **right frontopolar cortex**. The last one is also involved for case B. Both A and B show some disruption, even though at different degree, of the connectivity between the right pars opercularis and the cingulate cortex. Studies on EEG for PD patients in resting state focus on the effects on right pars opercularis and the left insula [49], in correlation with anxiety symptoms of the disease. Furthermore, cases A and B reveal a variation of connectivity between the **dorsal anterior cingulate cortex** and the **ventral anterior cingulate cortex**. Concerning the anterior cingulate cortex, the dorsal part is more related to cognition, while the ventral part is more connected to emotion. Thus, the effects of connectivity variations in these regions for PD patients provoke neuropsychiatric symptoms and motor symptoms [50]. In the **temporal lobe**, both cases A and B show a connectivity diminution between the left superior temporal sulcus and the left auditory cortex, and an increase in connectivity between the right superior temporal sulcus and the left default mode network. Observing the action of the K-operator on the **parietal lobe**, we notice for both cases a decrease of connectivity between the left temporo-parietal junction and the left anterior intraparietal sulcus. In the **occipital lobe**, both A and B present a connectivity diminution between striate and right lateral occipital complex, and, concerning **subcortical** and other areas of the brain, an increase of connectivity between basal ganglia and right insula. Hyperactivity of basal ganglia, also in clusters including cerebellum, insula, thalamus, has been proved for Parkinson's disease patients [51].

6 Conclusions and future research

We started our research with the conceptual model of neurological disease as the effect of a mathematical operator, the K-operator, acting on the brain network and altering the weights of their connections. We considered data from a medical dataset, PPMI, on Parkinson's Disease, and we experimentally computed a numerical-matrix expression for the K-operator.

Summarizing, we presented two case studies. We started from the fMRI of a healthy control and the fMRI of a patient affected by PD, considering the second as the result of the action of K on the healthy brain. We also wrote the K-operator as the tensor product of the submatrices acting on each brain lobe. Observing the values of the submatrices, we confirmed some of the findings of [21], a statistical study on the same dataset, where the brain networks of a number of healthy control patients were compared against PD patients. Concerning the PD patient, in our study we considered his fMRI at a certain follow-up in the dataset. Conceptually, the patient has been "photographied" at a certain time point of the disease progression. For this reason, we developed a second case study, for a first approach on the time evolution of the K-operator. We focused on the same PD patient, a female of 56 years old, analyzing her fMRI at the baseline and at the first follow-up, 1 year later. We retrieved results from the literature, in particular concerning dorsolateral prefrontal cortex [38], dorsolateral prefrontal cortex and frontopolar cortex [39], intraparietal sulcus [41], Broca's area, temporo-parietal junction [40], cingulate cortex [44], and intraparietal sulcus [43]. Both our case studies presented a variation of connectivity between the dorsal anterior cingulate cortex and the ventral anterior cingulate cortex, and in the occipital lobe, and a hyperactivity of basal ganglia and insula. Also, these joint results confirm findings from the medical literature. In particular, EEG-based studies on PD patients in resting state show neuropsychiatric effects, mainly anxiety in relation to connectivity variation on right pars opercularis and left insula [49], and cognitive alterations in relation with the dorsal cingulate cortex [50]. Also, the pathways between ganglia and thalamus are disrupted in Parkinson's Disease patients [51]. Considering in more detail the limbic system and its interaction with other areas of the brain, we confirmed the increase of connectivity between the cerebellum and ventral tegmental area for PD patients, as reported in the literature [36]. We also run a preliminary comparison between the K-operator representing the transition from a healthy brain to a diseased brain for different diseases, highlighting the differences, especially concerning ventral tegmental area, substantia nigra, and nucleus accumbens. As a general remark, a detailed analysis of dopaminergic circuits, and the brain network re-wiring in the case of dopaminergic pathways dysfunctions, can shed light on common mechanisms underlying different diseases such as PD, schizophrenia, and mood disorders (e.g., depression)

[37], where dopamine plays a major role. In this framework, a detailed analysis with the K-operator can point toward similarities and differences across diseases.

We also computed the K^{-1}, as a "healing" operator reversing the effects of K. Such an approach may provide hints about the brain-network regions toward which the therapy, being it surgical or pharmacological, could be specifically addressed. Of course, this typology of information should be tested on a great number of brain networks, to take into account gender-based, age-based, and individual differences of brain-network fine-graining organization. This information should also be added to the existing physicians' knowledge. Further research may be focused on the refinement of a time-dependent K-operator, which may be computed on an average of multiple patients at each time point. An ambitious perspective would also be the function approximation of the elements of $K(t)$. The computation of the K-operator between multiple pairs of consecutive connectivity matrices for the same PD patient can help confirm the information on the dynamic progression of the disease, but also, from a mathematical point of view, would allow us to approximate a time-depending version of the K-operator. Such a study, developed for different patients with the same disease, may allow one to improve the approximation of the K-operator for the considered disease. From the analysis of K^{-1}, we can focus on the ROIs that have to be targeted by therapies. Comparing the effects of existing drugs, it is possible to hypothesize a new drug combination to extend the healing effect to those areas not addressed yet, but that should, according to K. This idea is to be developed in further research, more physiology-based, also including perturbative variation on the action of an existing drug, approximating a better healing.

While in this research, we focused on the first matrices of the fMRI series, in a following study, we can consider the transition from the first to the last one for each time point of the patient, and also include in our analysis the non-diagonal blocks of the K-operator. Future research developments can also include the analysis of experimental data on disease induction on *in vitro* cells and simulation of their development through *in silico* techniques. Such an approach may help us infer the characteristics of damage induction at a higher level of the network, avoiding invasive experimental techniques. A search for commonalities in K-operators for different diseases may foster a more general, theoretical approach (as wished in [19]). Ultimately, paradigms and methods of theoretical physics can help understand nature, including that part of nature that we use to understand physics: our own minds.

Acknowledgements This article was developed within the project funded by Next Generation EU—"Age-It–Ageing well in an ageing society" project (PE0000015), National Recovery and Resilience Plan (NRRP)—PE8—Mission 4, C2, Intervention 1.3. The views and opinions expressed are only those of the authors and do not necessarily reflect those of the European Union or the European Commission. Neither the European Union nor the European Commission can be held responsible for them.

Funding Open access funding provided by Consiglio Nazionale Delle Ricerche (CNR) within the CRUI-CARE Agreement.

Data availability We analyzed data from the Parkinson's Progression Markers Initiative (PPMI) with the following licenses and restrictions: "Investigators seeking access to PPMI data must sign the Data Use Agreement, submit an Online Application and comply with the study Publications Policy. Requests to access these datasets should be directed to PPMI, https://ida.loni.usc.edu/collaboration/access/appLicense.jsp."
Further data have been driven from the ADNI dataset, that is, the Alzheimer's Disease Neuroimaging Initiative (ADNI) database (https://adni.loni.usc.edu). According to the guidelines, we state that "as such, the investigators within the ADNI contributed to the design and implementation of ADNI and/or provided data but did not participate in the analysis or writing of this report. A complete listing of ADNI investigators can be found at: https://adni.loni.usc.edu/wp-content/uploads/how_to_apply/ADNI_Acknowledgement_List.pdf."

Declarations

Codes availability The original Python-Jupyter code can be accessed from GitHub, at https://github.com/medusamedusa/K_operator_parkinson. Part of the code, concerning visualization, has been adapted from the GNN tutorial by Sidney Hough, Julian Quevedo, and Pino Cholsaipant. Their original code, described in [30], developed as part of their Stanford CS224W course project, can be retrieved at https://colab.research.google.com/drive/16pZ3j3WZ5_E1oUa_70uz5Xb4ZVqHokMJ?usp=sharing.

References

1. M.E.J. Newman, SIAM Rev. **45**(2), 167 (2003)
2. S. Guo, X. Chen, Y. Liu, R. Kang, T. Liu, D. Li, Front. Phys. **9**, 698077 (2021)
3. A.A. Toffano, G. Chiarot, S. Zamuner, M. Marchi, E. Salvi, S.G. Waxman, C.G. Faber, G. Lauria, A. Giacometti, M. Simeoni, Sci. Rep. **10**, 17930 (2020)
4. M.P. van den Heuvel, O. Sporns, Trends Cogn. Sci. **12**(12), 683 (2013)
5. G. Schummer, Biofeedback (2009). https://web.archive.org/web/20150907181212/http://www.resourcenter.net/images/AAPB/Files/Biofeedback/2008/biof-36-04-157-162.pdf
6. F. Corrivetti, G. Herbet, S. Moritz-Gasser, H. Duffau, World Neurosurg. **97**, 756.e1 (2017). https://doi.org/10.1016/j.wneu.2016.10.025
7. M.P. van den Heuvel, R.C. Mandl, C.J. Stam, R.S. Kahn, H.E.H. Pol, J. Neurosci. **30**(47), 15915 (2010)
8. J. Sawicki, E. Schöll, ArXiV (2024). https://doi.org/10.48550/arXiv.2401.17988
9. J. Royer, B.C. Bernhardt, S. Larivière, E. Gleichgerrcht, B.J. Vorderwülbecke, S. Vulliémoz, L. Bonilha, Epilepsia **63**, 537 (2022)
10. F. Bartolomei, M. Guye, F. Wendling, EPJ Nonlinear Biomed. Phys. **1**(4), 1 (2013)
11. C. Lainscsek, P. Salami, V. Rezende Carvalho, E.M.A.M. Mendes, F. Miaolin, S.S. Cash, T.J. Sejnowski, Chaos **33**(123136) (2023)
12. P. Barone et al., *Neurol. Clin.* (Idelson - Gnocchi, Naples, 2021)
13. R. Tripathi, B.J. Gluckman, Front. Netw. Physiol. **2**, 911090 (2022)
14. K. Lehnertz, T. Bröhl, R. Randi von Wrede, Neurobiol. Dis. **181**, 106098 (2023)
15. B. Lucci, The Italian Journal of Neurological Sciences p. 49 (1998)
16. A. Fathian, Y. Jamali, M. Raoufy et al., Sci. Rep. **12**, 14998 (2022). https://doi.org/10.1038/s41598-022-18987-y
17. A. Badhwar, A. Tam, C. Dansereau, P. Orban, F. Hoffstaedtre, P. Bellec, Alzheimer & Dementia **8**, 73 (2017)
18. H. Cui, W. Dai, Y. Zhu, X. Li, L. He, C. Yang, in Medical Image Computing and Computer Assisted Intervention - MICCAI 2022, Lecture Notes in Computer Science, vol. 13438, ed. by L. Wang, Q. Dou, P.T. Fletcher, S. Speidel, S. Li (Springer, Cham, 2022), Lecture Notes in Computer Science, vol. 13438. https://doi.org/10.1007/978-3-031-16452-1_36
19. W.W. Seeley, Cold Spring Harb Perspect. Biol. **9**(a023622) (2017). https://cshperspectives.cshlp.org/content/9/8/a023622.full.pdf
20. M. Mannone, P. Fazio, N. Marwan, Chaos **34**(5) (2024). https://doi.org/10.1063/5.0199988
21. B. M., E.G. Keeling, N.J. Ray, A. Macerollo, M. Silverdale, A.M. Stokes, Front. Neurol. **14**, 1137780 (2023). https://doi.org/10.3389/fneur.2023.1137780
22. R.B. Buxton, Reports on Progress in Physics **76**(9) (2013)
23. S. Sandrone, M. Bacigaluppi, M.R. Galloni, S.F. Cappa, A. Moro, M. Catani, M. Filippi, M.M. Monti, D. Perani, G. Martino, Brain **137**(2), 621 (2014)
24. D. of Medical Physics University of Wisconsin School of Medicine, P. Health. Functional Magnetic Resonance Imaging (fMRI) . https://medphysics.wisc.edu/research/fmri/functional-magnetic-resonance-imaging-fmri/, page accessed 3 June 2024
25. J.J. Medina, Psychiatric Times **26**(4) (2009)
26. X. Li, P.S. Morgan, J. Ashburner, J. Smith, C. Rorden, J. Neurosci. Methods **264**, 47 (2016)
27. G. Varoquaux, A. Gramfort, F. Pedregosa, V. Michel, B. Thirion, Information processing, in *Medical imaging (IPMI 2011)*. ed. by G. Székely, H. Hahn (Springer, Cham, 2011), pp.562–573
28. J.A. Kiernan, N. Rajakumar, Barr: Il Sistema Nervoso dell'Uomo (EdiSes, 2015)
29. E.T. Rolls, C.C. Huang, C.P. Lin, J. Feng, M. Joliot, Neuroimage **206**, 116189 (2020). https://doi.org/10.1016/j.neuroimage.2019.116189
30. S. Hough, GNNs in neuroscience: graph convolutional networks for fMRI analysis. https://medium.com/stanford-cs224w/gnns-in-neuroscience-graph-convolutional-networks-for-fmri-analysis-8a2e933bd802 (2022, accessed on 3 June 2024)
31. M. Shinohara, K. Yokoi, K. Hirayama, S. Kanno, Y. Hosokai, Y. Nishio, T. Ishioka, M. Otsuki, A. Takeda, T. Baba, M. Aoki, T. Hasegawa, A. Kikuchi, W. Narita, E. Mori, K. Suzuki, PLoS ONE **14**(e0279007), 12 (2022)
32. J.U. Henschke, J.M.P. Pakan, Front. Syst. Neurosci. **17**(1165307) (2023)
33. H.H. Sun, J.B. Hu, J. Chen, X.Y. Wang, X.L. Wang, P.L. Pan, C.F. Liu, Front Neurosci. **4**(14) (2020)
34. J. Dick, J. Fredrick, G. Man, J.E. Huber, J. Lee, Clin. Linguist. Phon. **32**(9), 804 (2018)
35. F. Blandini, G. Nappi, C. Tassorelli, E. Martignoni, Prog. Neurobiol. **62**(1), 63 (2000)
36. V.P. Murty, M. Shermohammed, D.V. Smith, R.M. Carter, S.A. Huettel, R.A. Adcock, Neuroimage **100**, 580 (2014)
37. I.M. O'Shea, H.S. Popal, I.R. Olson, *et al.*, Sci Rep **12**(3289) (2022). https://doi.org/10.1038/s41598-022-07020-x
38. H. Srovnalova, R. Marecek, R. Kubikova, I. Rektorova, Exp. Brain Res. **223**(2), 251 (2012). https://doi.org/10.1007/s00221-012-3255-9
39. X. Jia, W. Fan, Z. Wang, Y. Liu, Y. Li, H. Li, H. Li, T. Ma, J. Wang, Q. Yang, Front Aging Neurosci. **10**(13), 750767 (2022)
40. B.A. Pickut, W. Van Hecke, E. Kerckhofs, P. Mariën, S. Vanneste, P. Cras, P.M. Parizel, Clinical Neurology and Neurosurgery **115**(12), 2419 (2013). https://www.sciencedirect.com/science/article/pii/S0303846713004083

41. M. Arioli, Z. Cattaneo, M.L. Rusconi, F. Blandini, M. Tettamanti, Neuroimage Clin. **35**, 103031 (2022). https://doi.org/10.1016/j.nicl.2022.103031
42. R.S. Weil, A.E. Schrag, J.D. Warren, S.J. Crutch, A.J. Lees, H.R. Morris, Brain **139**(11), 2827 (2016)
43. C. Sasaki, K. Yokoi, H. Takahashi, T. Hatakeyama, K. Obara, C. Wada, K. Hirayama, Psychogeriatrics **22**(1), 38 (2022). https://doi.org/10.1111/psyg.12771
44. B.A. Vogt, Handb. Clin. Neurol. **166**, 253 (2019). https://doi.org/10.1016/B978-0-444-64196-0.00013-3
45. C.J. Stoodley, E.M. Valera, J.D. Schmahmann, Neuroimage **59**(2), 1560 (2012)
46. L.J. Altmann, M.S. Troche, Parkinson's Dis. **1** (2011)
47. P.E. Mosley, G.A. Robinson, Brain **146**(7), 2661 (2023). https://doi.org/10.1093/brain/awad180
48. L.A. Morris, S.J. Harrison, T.R. Melzer, J.C. Dalrymple-Alford, T.J. Anderson, M.R. MacAskill, C.J. Le Heron, Brain **3**(146), 2739 (2023). https://doi.org/10.1093/brain/awad113
49. N. Betrouni, E. Alazard, M. Bayot, G. Carey, P. Derambure, L. Defebvre, A.F.G. Leentjens, A. Delval, K. Dujardin, Neurophysiol. Clin. **52**(3), 202 (2022)
50. M. Banwinkler, H. Theis, S. Prange, T. van Eimeren, Brain Sci. **12**(9), 1248 (2022)
51. V. Filyushkina, V. Popov, R. Medvednik, V. Ushakov, A. Batalov, A. Tomskiy, I. Pronin, A. Sedov, Front. Neurol. **7**(10), 847 (2019)